Effect of Temperature, pH and Shell Thickness on the Rate of Mg^{2+} and Ox^{2-} Release from Multilayered Polyelectrolyte Shells Deposited onto Microcrystals of Magnesium Oxalate

A. I. Petrov, A. V. Gavryushkin,[†] and G. B. Sukhorukov*[,‡]

Institute of Theoretical and Experimental Biophysics, Russian Academy of Sciences, 142290 Pushchino, Moscow Region, Russia, State Research Center of Applied Microbiology, 142179 Obolensk, Moscow Region, Russia, and Max Planck Institute of Colloids and Interfaces, 14424 Potsdam/Golm, Germany

Received: April 24, 2002; In Final Form: September 8, 2002

The influence of temperature and pH on the rate of dissolving the naked magnesium oxalate microcrystals and the microcrystals coated with multilayered polyelectrolyte shells of different thickness and molecular composition—$(PAH-PSS)_n$ and $(PAH-PSS)_nPAH$, where $n = 0$, 5, 10, and 15 was studied by a conductometry technique. Only shells with $n > 10$ were found to noticeably slow the release rate of magnesium and oxalate (Ox^{2-}) ions out of polyelectrolyte microcapsules, and the effect increases with n. The estimated lower value for the diffusion coefficient of Mg^{2+} and Ox^{2-} transport across the walls of polyelectrolyte shells is approximately equal to 10^{-9} cm^2/s, which is about four orders lower than that for free diffusion of Mg^{2+} and Ox^{2-} in water solutions, but two orders higher than the diffusion coefficient for transport of low molecular weight organic substances (MW $\sim$ 400) through the polyelectrolyte shells. No effect of pH in the range from 4.5 to 9.0 was revealed on the permeability of multilayered polyelectrolyte microcapsules made of PSS and PAH relative to magnesium and oxalate ions. To the contrary, raising the temperature results in an essential increase in the rate of Mg^{2+} and Ox^{2-} release from the shells, manifesting itself in a more than 2-fold increase of the diffusion coefficient in the temperature range 20−50 °C.

Introduction

The controlled release of different substances at the given site, time, and with a determined rate is the challenging task in medicine, chemistry, agriculture, industry, cosmetic and food technologies, and many other fields. The solution of the problem has usually involved searching for a way of their packing into polymeric microcapsules with appropriately optimized wall properties.[1−8] The release of encapsulated core substances into their surroundings is achieved either by direct disruption of polymeric shells in some way, for instance, mechanical, chemical, biological degradation, the exposure to physical factors such as heat, electromagnetic irradiation of different wavelength and others, or by subtly managing the permeability of microcapsule walls while retaining their overall integrity. Therefore, much attention has been paid not only to the elaboration of microencapsulation technologies, but also to designing the polymer coatings with predetermined and controllable physicochemical properties.

Recently, a new approach to the microencapsulation of different materials based on the alternating adsorption of oppositely charged polyelectrolytes onto colloid-sized microparticles has been put forward[9−11] (for a review, see ref 12). It can be considered as an extension of the "layer-by-layer" or "electrostatic self-assembly" (ESA) technology invented by G. Decher and J. D. Hong[13,14] in the early 1990s and recognized now as an intriguingly simple but extremely versatile method for designing nanocomposite multilayered polyelectrolyte films (see reviews in refs 15−17). The possibility of wide variation of different combinations of polyelectrolyte pairs and many other charged entities, purposeful chemical modification of starting materials, as well as unique alternating packing of positively and negatively charged polyelectrolyte layers open great wealth of ways for manipulating the properties both of flat polyelectrolyte films[18−26] and of microcapsules,[9−12,27−30] including the permeability of their walls.

Despite rather limited data on the relationship between the chemical nature of constituents and properties of multilayer polyelectrolyte microcapsules—most of the studies have been done on the microcapsules made of poly(allylamine hydrochloride), PAH, and poly(styrene sulfonate), PSS—the results revealed high sensitivity of multilayered polyelectrolyte shells to subtle changes in surroundings. In particular, it was demonstrated that pH can play the role of a trigger switching off and on between "open" and "closed" states of polyelectrolyte shells, thus enabling the effective control over their release properties.[27,28] pH changes and the assembly of a lipid bilayer on the surface of multilayered polyelectrolyte microcapsules as another approach to affect the porosity of their walls allow controlled release of microencapsulated substances ranging from low molecular weight organic molecules (such as 6-carboxyfluorescein, MW $\sim$ 376) to high molecular weight polymers (dextran, MW $\sim$ 2 000 000).[27−31] It is well documented now that the walls of multilayered polyelectrolyte microcapsules have porous structure providing more or less delayed release kinetics for low molecular weight organic molecules.[11,29,32,33] However, there are practically no data about the release properties of multilayered polyelectrolyte microcapsules relative to such small entities as inorganic ions, though a specificity and selectivity of ion transport across *flat* multilayered polyelectrolyte films has been recently demonstrated.[34−36]

In the present work, we describe the release properties of multilayered polyelectrolyte microcapsules made of PAH and

* Corresponding author.
[†] State Research Center of Applied Microbiology.
[‡] Max Planck Institute of Colloids and Interfaces.

10.1021/jp026007f CCC: $25.00
Published on Web 12/24/2002

PSS relative to Mg^{2+} and oxalate ions and the factors affecting the kinetics of this process. The electric conductivity approach was used to monitor the rate of dissolving the free magnesium oxalate microcrystals and the same microcrystals covered with different number of polyelectrolyte layers. The choice of magnesium oxalate was determined by its solubility characteristics proper for deposition of polyelectrolyte shells (see Experimental Section).

Experimental Section

Materials. *Chemicals.* Sodium poly(styrene sulfonate), PSS, MW ~ 70 kDa, and poly(allylamine hydrochloride), PAH, MW ~ 15 kDa, were obtained from Aldrich and used without additional purification. Magnesium chloride hexahydrate, $MgCl_2 \cdot 6H_2O$, and ammonium oxalate monohydrate, $(NH_4)_2C_2O_4 \cdot H_2O$, (Reakhim, Russia) of reagent grade qualification were used as received. Because of high hygroscopicity of $MgCl_2 \cdot 6H_2O$ this salt was stored in a desiccator over P_2O_5. Double quartz distilled water was used in all experiments.

Microcrystals of $MgC_2O_4 \cdot 2H_2O$. The microcrystals of magnesium oxalate, $MgC_2O_4 \cdot 2H_2O$ with narrow size distribution (1−3 μm) were prepared through a controlled crystallization initiated by rapid mixing of $MgCl_2 \cdot 6H_2O$ and $(NH_4)_2C_2O_4 \cdot H_2O$ solutions resulting in supersaturation with respect to MgC_2O_4. The degree of supersaturation (SSD) can be expressed as follows: $SSD = [Mg^{2+}] \cdot [C_2O_4^{2-}]/K_{sp}$, where the numerator is the product of concentrations of Mg^{2+} and $C_2O_4^{2-}$ ions just after mixing of $MgCl_2$ and $(NH_4)_2C_2O_4$ solutions, and the denominator, K_{sp} ,is the solubility product of MgC_2O_4. Aliquots (25 μL) of reaction mixture (suspension of microcrystals) were taken every 5 min and analyzed under a light microscope. After reaching the necessary dimension of microcrystals, the reaction was stopped by rapid filtration through a membrane filter followed by thorough washing with cold water. The microcrystals thus obtained were dried in air at 50 °C.

Methods. *Polyelectrolyte Shell Deposition.* The multilayer assembly of oppositely charged polyelectrolytes was accomplished by sequential adsorption of PAH and PSS onto $MgC_2O_4 \cdot 2H_2O$ microcrystals. Typically, 10 mL of polyelectrolyte solution (concentrated 1 mg/mL) in 10 mM NaCl, pH 7.0, saturated with MgC_2O_4, was added to 25 mg of dry $MgC_2O_4 \cdot 2H_2O$ microcrystals (the resulting particle concentrated 0.25%, w/w) in a centrifuge tube and the suspension was gently shaken on a microshaker for 15 min. Then the suspension was centrifuged at 700 g for 10 min and the precipitate was washed three times with 10 mL of saturated solution of $MgC_2O_4 \cdot 2H_2O$, pH 7.0. To prevent particle aggregation, a short ultrasonic pulse was applied after each centrifugation step to the precipitate with newly added washing or polyelectrolyte solution. The same procedure was repeated with polyelectrolyte of opposite charge, resulting finally in the desirable number of deposited polyelectrolyte layers. It should be underlined once more that all steps of polyelectrolyte film deposition onto $MgC_2O_4 \cdot 2H_2O$ microcrystals were performed in solutions saturated with magnesium oxalate (concentrated ~0.5 mM) to prevent the dissolving of core particles.

Conductometry. The rates of dissolving the $MgC_2O_4 \cdot 2H_2O$ microcrystals covered with different number of polyelectrolyte layers—$(PAH-PSS)_n$ and $(PAH-PSS)_nPAH$, where $n = 0$, 5, 10, and 15—were measured by conductometry technique benefiting from the obvious increase in the electrical conductivity due to the release of magnesium and oxalate ions into the bulk solution. A conductivity meter OK-102/1 (Radelkis, Hungary) with a platinum electrode calibrated by standard KCl solutions was used in this study. A water-jacketed 50 mL measuring cell supplied with regulated magnetic stirrer and sensitive thermosensor provided for homogeneous mixing excluding the gradients of concentrations and temperature in the solution. The temperature was regulated with an ultrathermostat circulating the water with fixed temperature through the water jacket of the measuring cell.

Light Microscopy. A microphotometric setup on the basis of a light microscope MBI-11 (LOMO, Russia) supplied with digital photo- and videocamera on-line with a personal computer was used for visualization of $MgC_2O_4 \cdot 2H_2O$ microcrystals and for analysis of their size distribution. A simple home-made microelectrophoretic system was used for estimating the sign of the charge and the sign and value of the ξ-potential from the measured electrophoretic mobility of covered and uncovered $MgC_2O_4 \cdot 2H_2O$ microparticles.

Data Evaluation. For the quantitative analysis of the experimental data on the kinetics of dissolving the "naked" microcrystals of $MgC_2O_4 \cdot 2H_2O$ and those covered with a different number of polyelectrolyte layers, the simplified approach based on the theory of heterogeneous chemical reactions was used according to which the dissolving of solids is treated as physical diffusion through a thin layer adjacent to the surface.[37−39] The following assumptions are accepted: (i) the layer with thickness δ_o is stationary, that means the absence of any solvent flows within this layer even upon mixing of the solution; and (ii) there exists a linear gradient in concentration of dissolving substance through the layer, which in combination with Fick's first law of diffusion results in the following expression for the flux (j) of dissolving substance:

$$\frac{\partial M}{S\,\partial t} = j = -D\frac{C_s - C}{\delta_o} = -k(C_s - C) \qquad (1)$$

where M is the total mass of dissolving particles, S is their total surface area, t *is* time, D is the diffusion coefficient, δ_o is the thickness of the diffusional layer, C_s is the solubility of the substance (saturation concentration), C *is* the current concentration in bulk solution, and $k = D/\delta_o$ is the so-called permeability coefficient.

Simple transformation of eq 1 leads to the basic equation:

$$\frac{\partial C}{\partial t} = k\frac{S}{V_o}(C_s - C) \qquad (2)$$

where V_o is the volume of the solution. The peculiarities of its application to the analysis of dissolving kinetics of the "naked" and covered $MgC_2O_4 \cdot 2H_2O$ microparticules is discussed in the next section.

Results and Discussion

$MgC_2O_4 \cdot 2H_2O$ Microcrystals and Polyelectrolyte Shell Self-Assembly. The microcrystals of magnesium oxalate used as core particles for deposition of multilayered polylectrolyte films were prepared by a controlled crystallization from supersaturated relative to MgC_2O_4 solutions created by mixing of relatively high concentrations of magnesium chloride and ammonium oxalate solutions. The nucleation step, i.e., the formation of primary centers of crystallization, was found not only to be the rate-limiting process but also to determine essentially the quality of obtained microcrystals (the homogeneity in habit and size). Thus, the nucleation rate (regulated by application of ultrasonic pulse of different duration), the initial degree of supersaturation, SSD (usually SSD ≈ 50 was created,

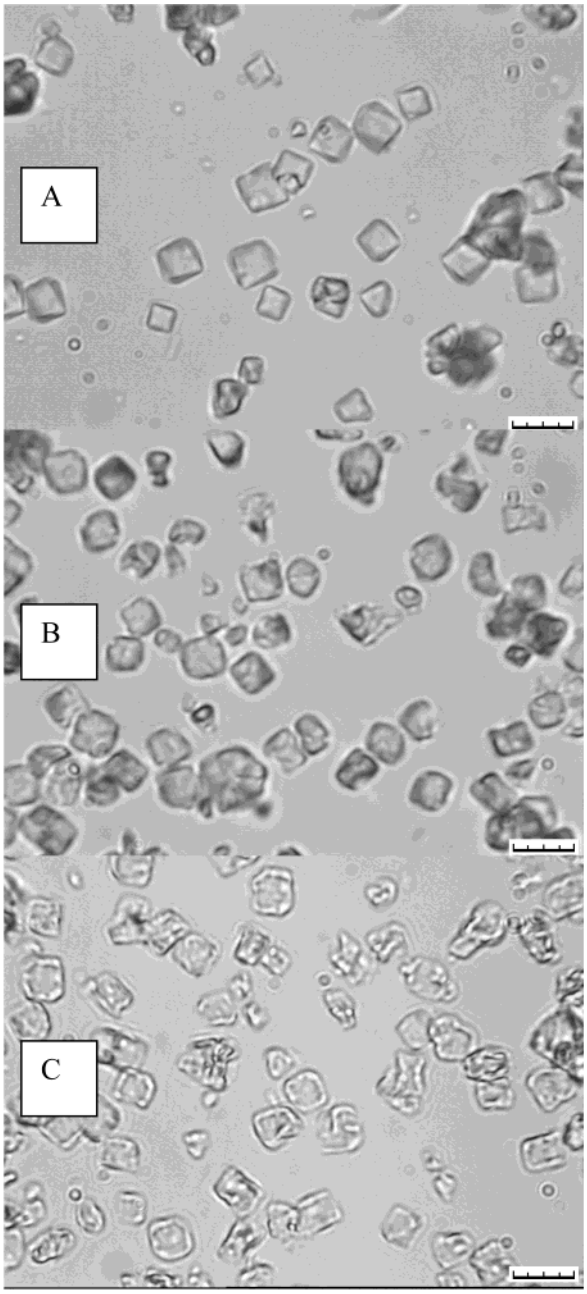

Figure 1. Light microscopic image of one sample of magnesium oxalate microcrystals (A), the same microcrystals coated with $(PAH-PSS)_{15}$ multilayered polyelectrolyte shells (B), and the hollow shells obtained by core dissolving in EDTA solution (C). The scale bar corresponds to 4 μm.

with equimolar ratio of magnesium chloride and ammonium oxalate), and the time were the main variable parameters which when appropriately chosen result in desirable uniform microcrystals of $MgC_2O_4 \cdot 2H_2O$ with narrow size distribution (Figure 1A). Among different approaches used to quantify the size distribution of irregular colloidal particles,[40] the so-called "projected area diameter (d_a)" approach seems to be the most adequate for sizing rather uniform rhomboidal microcrystals of $MgC_2O_4 \cdot 2H_2O$. In this approach, a circle is overlapped with the particle image on the light or electron micrograph and the diameter of the circle is varied to get the best matching of two areas—the circle area and the projected area of the microparticle. The diameter, d_a, of the circle is then taken as the diameter of the sphere, which approximates the real microparticle. A home-written image processing and analysis program for Microsoft Windows 95 was used to get the histograms of size distribution of $MgC_2O_4 \cdot 2H_2O$ microcrystals. The histograms of size distribution for two samples of $MgC_2O_4 \cdot 2H_2O$ microparticles are shown in Figure 2. It is remarkable that we have a rather narrow size distribution, and a common trend is the noticeable widening of size distribution histograms with an increase in the average diameter of particles determined from maximum of the histogram. This seems to be a general feature. The same trend in size distribution was observed by us upon the growth of spherical microcrystals of $CaCO_3$[41]—the smaller the microcrystals, the narrower their size distribution.

The microelectrophoretic measurements showed that $MgC_2O_4 \cdot 2H_2O$ microparticles bear total negative charge. The value of ξ-potential estimated from electrophoretic mobility, $u = 0.56 \times 10^{-8}$ m^2/V s, using the Smoluchowski equation, $\xi = u\eta/\epsilon$, where η and ϵ are the viscosity and dielectric permeability of the solution, respectively, is equal to -8 mV in 10 mM NaCl. Thus, the procedure of polyelectrolyte layer deposition was started with the polycation, PAH, and following the already classical repetition of the sequence of operations: first polyelectrolyte adsorption $\rightarrow$ triple washing $\rightarrow$ adsorption of polyelectrolyte of opposite charge, the multilayered polyelectrolyte shells of different thickness were deposited onto magnesium oxalate microcrystals (Figure 1B) Magnesium oxalate core particles, like the cores of $CaCO_3$ microspheres,[41] are easily dissolved in EDTA solutions, leaving the hollow multilayered polyelectrolyte shells (Figure 1C). A shrinkage of the shells is observed, evidencing some structural, at least at the level of morphology, rearrangements during the dissolving of core particles.

Dissolving Kinetics. The kinetics of dissolving the magnesium oxalate microcrystals, both naked and covered with polyelectrolyte shells of different thickness, was measured by a conductometry technique benefiting from the increase of the electric conductance of bulk solution due to release of magnesium oxalate in dissociated ionic form. Figure 3 demonstrates two kinetic curves for dissolving the naked magnesium oxalate microcrystals (upper curve) and the same microcrystals packed into $(PAH-PSS)_{15}$ shells (lower curve). An essential slowing down in the rate of dissolving is observed, pointing to the presence of a diffusional barrier revealed by polyelectrolyte shells relative to the transport across their walls of such small species as magnesium and oxalate ions.

We have measured the kinetics of dissolving the magnesium oxalate microcrystals at different temperatures, pH values, and the number of deposited polyelectrolyte layers. Some of these data are presented in the following three figures (Figures 4−6). Figure 4 shows the effect of temperature on the kinetics of dissolving the naked (Figure 4A) microcrystals of $MgC_2O_4 \cdot 2H_2O$ and those covered with $(PAH-PSS)_{15}$ shells (Figure 4B). It is seen that the rise in temperature exerts a pronounced effect on the release kinetics, increasing essentially the rate of dissolving the microcrystals. Indeed, the time of dissolving the same initial mass of microcrystals (1.8 mg/50 mL of H_2O) decreases from several tens of minutes at 20 °C to several minutes at 50 °C. It is true both for naked and polyelectrolyte-coated microcrystals of $MgC_2O_4 \cdot 2H_2O$, but one can see that the diffusional barrier for the transport of magnesium and oxalate ions through the polyelectrolyte shells is retained at least up to 50 °C.

The kinetic curves for dissolving the magnesium oxalate microcrystals coated with (PAH−PSS) shells at different pH values are presented in Figure 5. It can be seen that in the range of pH 4.5−9.0 there is a very small, if any, effect of

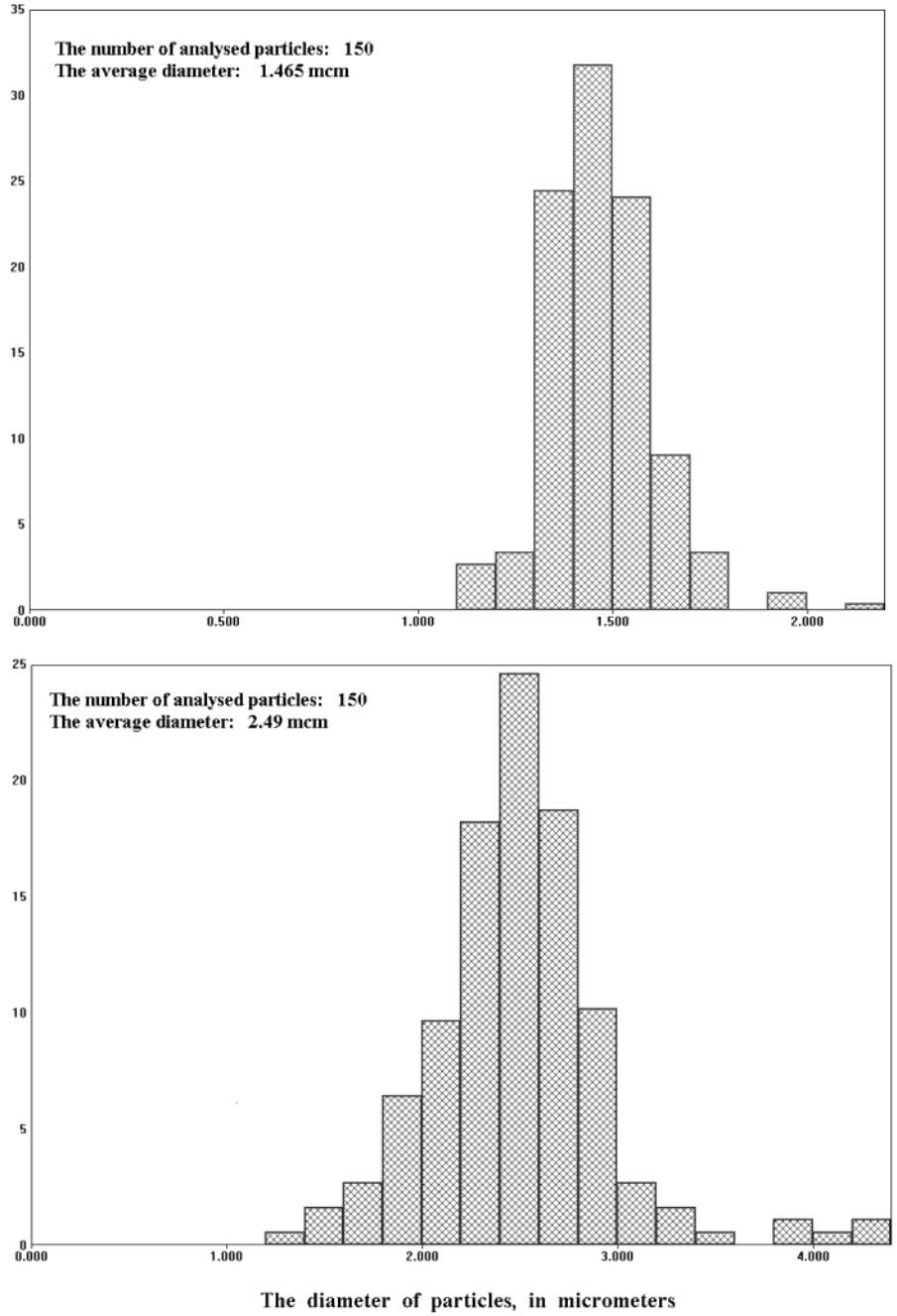

Figure 2. Histograms of size distribution for two samples of magnesium oxalate microcrystals. Top: histogram of the average diameter of microparticles (maximum at histogram) is about 1.5 μm, bottom: histogram of 2.5 μm.

polyelectrolyte shell on the rate of core dissolving. The result is unexpected in the light of well documented [27,28,32] sensitivity of $(PAH-PSS)_n$ polyelectrolyte shells to pH variations manifested in changes of their permeability to high molecular weight species such as proteins and dextrans as well as to low molecular weight dyes. Unfortunately, rather little is presently known about the intrinsic molecular structure of polyelectrolyte multilayers and the details of their structural rearrangements induced by pH changes in bulk solutions. It is not improbable that the character of structural rearrangements is dependent on the chemical nature of core particles, which may significantly influence the molecular mobility and rigidity of multilayers. One cannot exclude that in the case of magnesium oxalate microcrystals as core particles there are practically no pH-induced structural changes in the pH range 4.5−9, or that the scale of pH-induced changes in pore size of polyelectrolyte shell lies far away from the dimensions of such small entities as magnesium and oxalate ions and does not effect noticeably their travel across the shell. It should be kept in mind, also, that pores in multilayered polyelectrolyte shells may be essentially different from pores in lipid bilayers, being not direct "through-bilayer" but rather labyrinth-like canals and cavities, making the average distance of ions traveled inside polyelectrolyte multilayer much longer in comparison with shell thickness. Hence, more detailed information on the structure of polyelectrolyte shells and its change upon bas−-acid titration is necessary to understand the molecular mechanisms of the pH effect on their permeability relative to different species.

Figure 6 demonstrates the effect of polyelectrolyte shell thickness on the rate of dissolving the magnesium oxalate microcrystals. It is seen that only starting with $n > 10$, a retardation in the rate of dissolving the magnesium oxalate

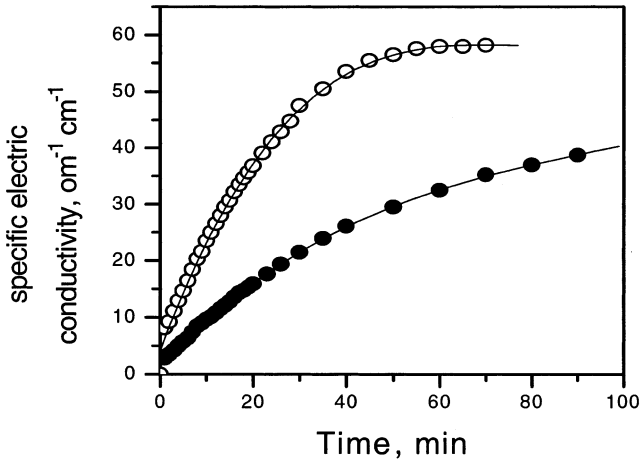

Figure 3. Kinetic curves of dissolving the naked (upper curve) microcrystals of magnesium oxalate, and the same microcrystals coated with $(PAH-PSS)_{15}$ polyelectrolyte shell (lower curve).

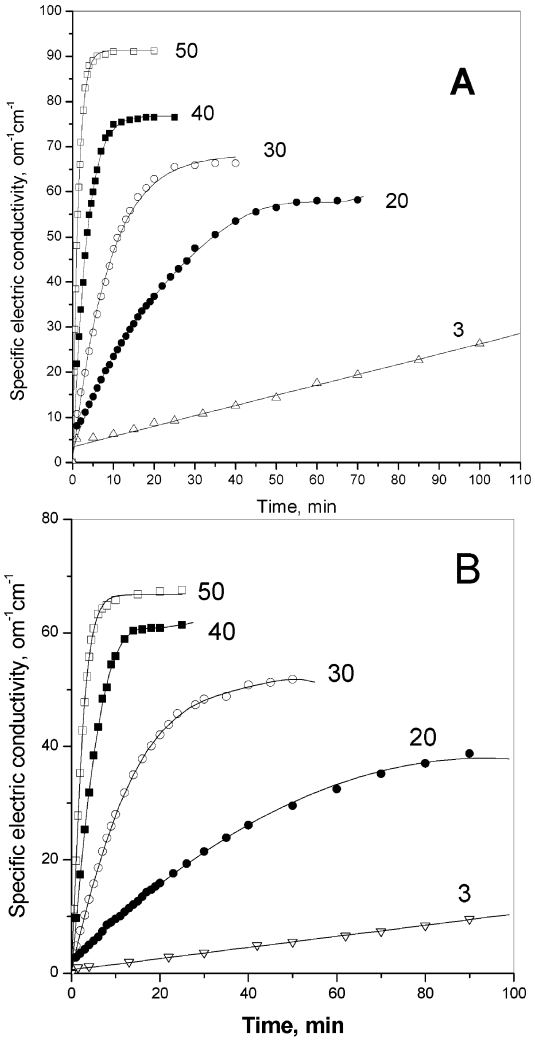

Figure 4. Effect of temperature on the kinetics of dissolving the naked (A) microcrystals of magnesium oxalate and those covered with $(PAH-PSS)_{15}$ polyelectrolyte shell (B). The numbers at curves show the temperature in °C.

microcrystals is observed. The thinner shells do not reveal barrier function detectable by conductometry technique relative to magnesium and oxalate ions.

Dissolving Model. The schematic representation of the dissolving model used for quantitative treatment of the above

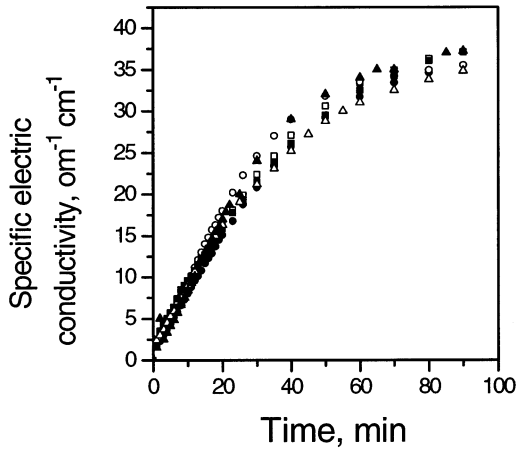

Figure 5. Kinetic curves of dissolving the magnesium oxalate microcrystal coated with (PAH−PSS) polyelectrolyte shell at different pH values in the range 4.5−9.0.

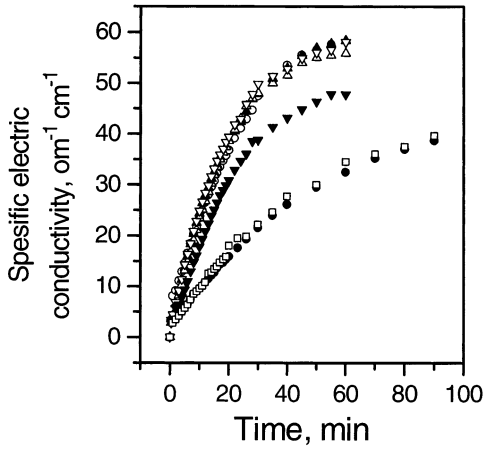

Figure 6. Effect of polyelectrolyte shell thickness on the kinetics of Mg^{2+} release: ○ naked magnesium oxalate microcrystals, ▲ $(PAH-PSS)_5$, ▽ $(PAH-PSS)_5$, △ $(PAH-PSS)_{10}$, ▼ $(PAH-PSS)_{10}PAH$, ● $(PAH-PSS)_{15}$, and □ $(PAH-PSS)_{15}PAH$.

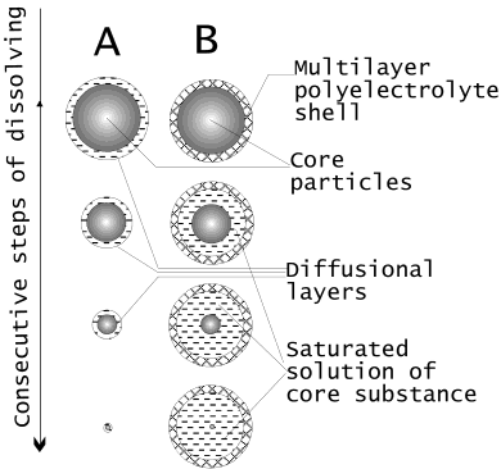

Figure 7. Schematic representation of the process of dissolving the naked magnesiun oxalate microcrystals (A) and those coated with a polyelectrolyte shell (B).

results is given in Figure 7. Column A refers to the naked magnesium oxalate microcrystals, and column B to those covered with multilayered polyelectrolyte shells. Two assumptions are made: (1) the real rhomboidal microcrystals of magnesium oxalate can be replaced by spheres with diameter corresponding to the maximum at the histograms of size

distribution, and (2) the concentration of magnesium oxalate inside polyelectrolyte shells is supported at the level of saturation at least at the initial stage of dissolving the core particles. While the former is a generally used approach to the estimation of the total surface area of disperse systems and seems to need no additional comments, the applicability of the latter is not obvious and should be discussed. The question is about the concentration of ions inside multilayered polyelectrolyte shell or, more exactly, in the vicinity of its inner surface. It looks quite natural that the slow rate of dissolving the bare magnesium oxalate microcrystals (Figure 3) will influence the concentration of ions inside the shells, and should be taken into account when analyzing the dissolution of core particles covered with polyelectrolyte shells. Moreover, it is tempting to consider one of two consecutive steps of the process (core dissolution and permeation of the products through the shell) as rate-limiting. For example, Gao et al.[42] give some experimental proofs that the core decomposition is the rate-limiting process at dissolution of melamine−formaldehyde particles, covered by a $(PSS/PAH)_8$ shell, in acidic medium. It may be true, however, for the initial stage of the process resulting in an accumulation of dissolving products inside polyelectrolyte shells. In a short time, the process inevitably reaches a steady-state regime after which the rates of core dissolving and permeation of products through the shell become equal. After setting up the steady-state conditions, the concentration of core dissolution products inside polyelectrolyte shells must reach a stationary level supported further by core dissolution. It can be shown that despite the seemingly low rate of dissolving the bare magnesium oxalate microcrystals (Figure 3), the concentration of Mg^{2+} and Ox^{2-} inside polyelectrolyte shells must rapidly reach the stationary level. Indeed, the rate of dissolving described by eq 2 is in reality the rate of accumulation of dissolving products in volume V_o, which is extremely small in the case of covered microcrystals, thus resulting in rapid (fractions of a second) setting up of the stationary concentration in the space between the inner surface of polyelectrolyte shells and the surface of core particles. Close proximity of polyelectrolyte shells to the surface of core particles makes it reasonable to approximate the stationary concentration of core dissolution products inside the shells by saturation concentration, C_s, of core substance, and this has been fruitfully used to quantitatively characterize the permeability of multilayered polyelectrolyte shells.[11,29,32,33]

What is the difference between the two cases presented in Figure 7? For the coated microparticles, we can assume S is equal to a constant at every moment of the dissolving process, while for the naked microparticles $S = S(t)$, which means that their total surface area changes (decreases) with dissolving. Then, the differential eq 2 may be integrated, taking into account the above remarks about the surface area of diffusion. Thus, after simple arithmetical transformations, we get the following expression (eq 5) for surface area of coated particles which is determined through the known experimental parameters:

$$S = 4\pi R_o^2 n \tag{3}$$

where R_o is the average radius of the particles determined from the histograms of size distribution, and n is the number of particles which can be easily found from the evident expression for the initial mass of particles (M_o) taken in the dissolving experiment:

$$M_o = \frac{4}{3}\pi R_o^2 \rho n \quad n = \frac{3M_o}{4\pi R_o^3 \rho} \tag{4}$$

where ρ is the density of magnesium oxalate.

Then the surface area of of particles may be expressed as follows:

$$S = 4\pi R_o^2 \frac{3M_o}{4\pi R_o^3 \rho} = \frac{3M_o}{R_o \rho} \tag{5}$$

And replacing S in eq 2 by its expression from eq 5, we get the differential equation with separatable variables

$$\frac{\partial C}{\partial t} = k\frac{3M_o}{V_o R_o \rho}(C_s - C) \tag{6}$$

which after integration gives a linear function with the slope angle dependent both on the rate constant of dissolving, k, and of known experimental parameters M_o, V_o, R_o, and ρ.

$$\ln\frac{1}{(1 - C/C_s)} = k\frac{3M_o}{V_o R_o \rho}t \tag{7}$$

The ratio of concentrations, C/C_s, in eq 7 may be replaced by the appropriate ratio of experimentally measured electric conductances, χ/χ_s, proceeding from the known expression for electric conductance of electrolyte solutions (eq 8) and taking into account that magnesium oxalate is an electrolyte of the 1:1 type, giving at dissociation equal concentrations of cations and anions, i.e., $C_i = C$:

$$\chi = \sum_i z_i^2 F^2 u_i C_i = C\sum_i z_i^2 F^2 u_i \tag{8}$$

where z_i is the charge of ion, F is the Faraday constant, u_i is the absolute mobility of ion, and C_i is the concentration of ions. Designating the ratio $\chi/\chi_s = K$, we come to the final form of eq 7:

$$\ln\frac{1}{(1 - K)} = k\frac{3M_o}{V_o R_o \rho}t \tag{9}$$

which was used for treatment of experimental kinetic curves of dissolving the polyelectrolyte-coated magnesium oxalate microcrystals. More complicated is the case with dissolving the naked microcrystals of magnesium oxalate for which, as it was pointed above, the surface area of dissolving particles is a function of time. But it is easy to show that eq 9 is applicable and for naked microcrystals, at least at the initial stage of the process.

Treatment of the Experimental Data. Thus, if the accepted model of dissolving is not too rough, the experimental curves of dissolving kinetics both for naked and polyelectrolyte-coated microcrystals of magnesium oxalate should be linearized in coordinates $\ln\{1/(1 - K)\}$ vs t, allowing us to determine the rate (or permeability) constant, k, which is, according to eq 1, directly connected with the diffusion coefficient. To validate the model, we have measured the dependence of kinetics of dissolving the magnesium oxalate microcrystals on the experimental parameters, M_o, V_o, and R_o. As an example, Figure 8 demonstrates the effect of M_o (Figure 8A) on the rate of dissolving the magnesium oxalate microcrystals, and the appropriate linearization of the kinetic curves (Figure 8B). Good linearization is achieved for the essential (initial) part of kinetic curves and the tangent of slope angles of these lines are linear functions of M_o (Figure 8C), in full agreement with eq 9. The same results were obtained upon variation of V_o and S_o. Moreover, as expected, the value of k is independent of variations in M_o, V_o, and S_o, and equals $9.0(\pm1) \times 10^{-4}$ cm/s

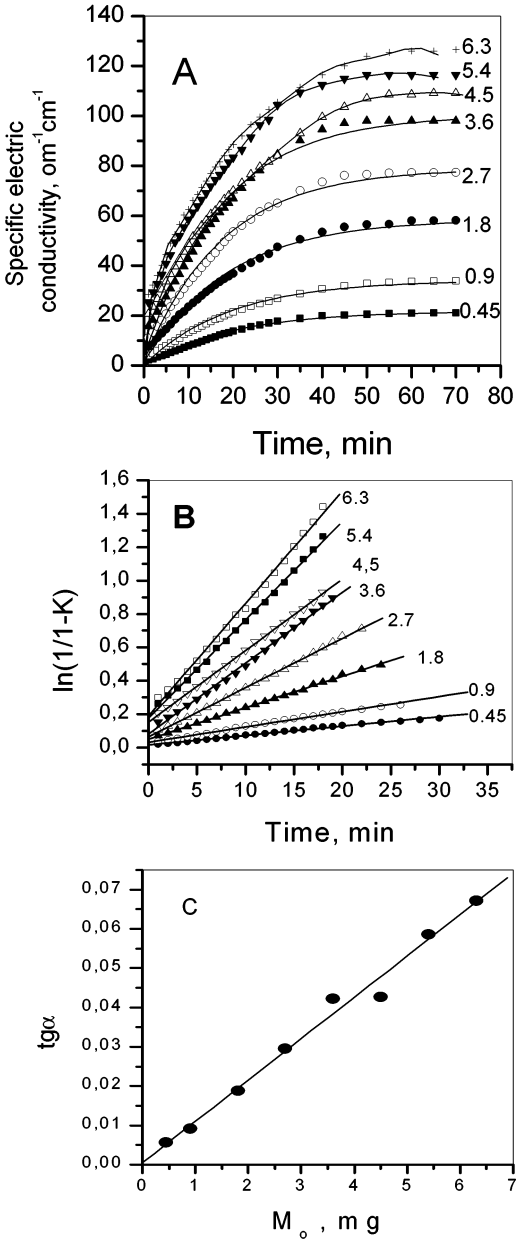

Figure 8. Effect of initial mass, M_o, on the rate of dissolving the naked microcrystals of magnesium oxalate with average radius 1.25 μm. (A) Kinetic curves of dissolving, (B) their linear anamorphoses built in accordance with eq 9 (see text), and (C) the dependences of tangent of slope angles of the lines on M_o. The numbers at curves designate the mass of magnesium oxalate microcrystals (mg) taken for dissolving in 50 mL of H_2O.

for naked magnesium oxalate microcrystals and 3.4($\pm$0.3) $\times$ 10^{-4} cm/s for those coated by $(PAH-PSS)_{15}$ and $(PAH-PSS)_{15}$PAH polyelectrolyte shells. Thus, one can conclude that the above model catches the main features of the dissolving process and gives rather realistic values of rate constant, *k*.

The kinetic curves (Figures 5−7) of dissolving the naked and covered with different number of polyelectrolyte layers magnesium oxalate microcrystals, obtained at different temperatures and pH values, are well linearized in coordinates ln $1/(1 - K)$ vs *t*, thus allowing us to determine the appropriate rate constants at different temperatutes and pH values from the slope angles. Very little scattering in slope angles is detected, evidencing the absence of any noticeable effect of pH on the rate of diffusion of magnesium and oxalate ions through the polyelectrolyte shell. The dependence of rate constant, *k*, calculated from the slope

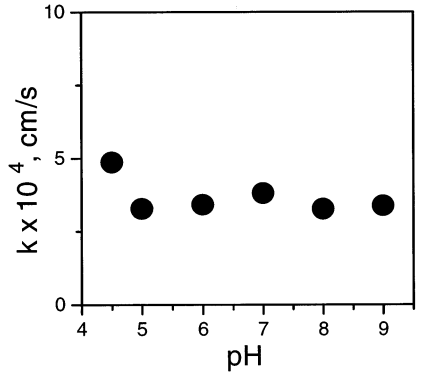

Figure 9. The dependence of rate constant, *k*, of dissolving the magnesium oxalate microcrystals coated with $(PAH-PSS)_{15}$ shells on pH.

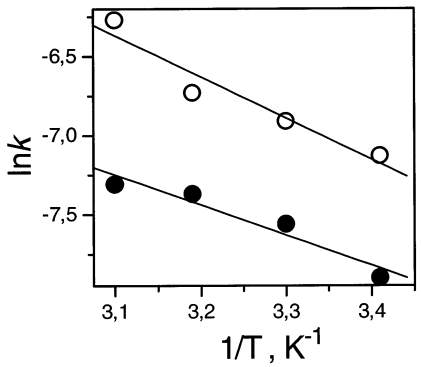

Figure 10. The Arrhenius plots of ln *k* *vs* inverse absolute temperature for dissolving the naked (upper) and coated with $(PAH-PSS)_{15}$ shells (lower) microcrystals of magnesium oxalate.

of the appropriate lines, on pH is presented in Figure 9. It is seen, that *k* values oscillate around 3.4($\pm$0.3) $\times$ 10^{-4} cm/s, and only at pH 4.5 does it noticeably exceed the average value. But this deviation from average seems to be apparent, because the process other than the release of magnesium and oxalate ions begins to contribute into measured electric conductance at acidic pH values, i.e., the protonation of oxalate anions at their release into bulk solution. As it follows from Figure 6, the noticeable effect of polyelectrolyte shells on Mg^{2+} and Ox^{2-} release is detected by conductometry technique only starting with $n > 10$. The value of *k* for $(PAH-PSS)_{15}$ and $(PAH-PSS)_{15}$ PAH shells calculated from the slope of appropriate lines equals 3.4($\pm$0.3) $\times$ 10^{-4} cm/s at 20 °C and depends strongly upon temperature. Figure 10 gives the Arrhenius plots of ln *k* vs inverse absolute temperature both for naked and coated with $(PAH-PSS)_{15}$ shells magnesium oxalate microcrystals. About 2-fold increase in *k* is observed in the temperature range 20−50 °C. The activation energies calculated from these plots egual 22 and 16 kJ/mol, respectively, for naked and coated microcrystals. These values fall into the range characteristic for diffusion-controlled heterogeneous processes.

It is possible, from the above data, to estimate the average diffusion coefficient for transport of Mg^{2+} and Ox^{2-} ions across the polyelectrolyte shells, taking into account the relation of *k*, diffusion coefficient *D*, and the thickness of diffusion layer, δ_o (see eq 1). In the case of polyelectrolyte-coated microcrystals, we can accept, according to ref 32, the thickness of one polyelectrolyte layer as 2 nm, resulting to $\delta_o \approx 30$ nm for $(PAH-PSS)_{15}$ and $(PAH-PSS)_{15}$ PAH shells, which gives the value of diffusion coefficient $D \approx 1 \times 10^{-9}$ cm^2/s. This value seems to give the lower limit for thediffusion coefficient of Mg^{2+} and Ox^{2-} travel through the (PAH−PSS) multilayer.

Taking into account an uncertainty in the thickness of polyelectrolyte layer accepted for calculations (2 nm for single polyelectrolyte layer accepted in this work after Antipov et al.,[32] or 3.4 nm measured by Qiu et al.[33]) the real value of *D* may surpass the above estimations nearly two times. An additional uncertainty in the estimated value of *D* may come from a simplified model used in this work for description of ion transport through the multilayered polyelectrolyte shells. The model proceeds from the gradient of chemical potential as the main driving force for diffusion, though it seems more adequate to consider the transport of any charged species through the multilayered polyelectrolyte shells as electro-diffusion directed by gradient of electrochemical potential. However, rather limited data on electrochemical properties of polyelectrolyte multilayers, their intrinsic structure and dynamics, and mechanisms of ion transport inside multilayers are available presently for development of a core-dissolving model taking into account the electrochemical phenomena. Hence, the simplified approaches to quantitation of the permeability properties of polyelectrolyte multilayers have been successfully used,[29,32,33,36,43,44] and the one described in this work gives rather realistic estimations for *D*, and may be useful in comparative analysis of polyelectrolyte shells permeability relative to different species. For example, the obtained value of *D* is four orders lower than the diffusion coefficient for free diffision of small ions in water solutions, but two orders higher than the diffusion coefficient for transport of low molecular organic substances, like carboxyfluorescein (MW $\sim$ 376), through the multilayered (PAH−PSS) shells.[32] It is interesting to note that the value estimated in this work of diffusion coefficient for Mg^{2+} and Ox^{2-} migration through the multilayered (PAH−PSS) shells falls in the range of *D* values for passive transport of alkali metal ions across natural biological membranes (10^{-8}−10^{-9} cm^2/s) found recently by Ersoz.[45]

Conclusions

The results presented in this work first demonstrated that the walls of multilayered polyelectrolyte microcapsules made of PAH and PSS reveal barrier functions not only relative to high molecular weight polymers—proteins, nucleic acids, polycarbohydrates, synthetic polymers, and relative to low molecular organic molecules, like dyes and drugs—but also to such small species as inorganic cations. That means that using different formulations of multilayered polyelectrolyte microcapsules, as well as by controlling the thickness of microcapsule walls, one can manage the rate of release of inorganic cations, which is of practical interest in many fields.

Acknowledgment. The work was supported by the Sofia Kovalevskaya Program of Alexander von Humbolt Foundations, German Ministry of Education and Research. Prof. Mohwald is greatly acknowledged for stimulating discussions. Prof. Dr. E. Donath (University of Leipzig) is appreciated for useful discussions and comments, Dr. A. Deev (ITEB, Puschino) for supplying the authors with an image analysis and processing program, and A. A. Antipov (MPI, Golm) for fruitful help and discussions.

References and Notes

(1) *Microspheres, Microcapsules & Liposomes*; Arshady, R., Ed.; Citus Books: London, 1999; Vol. 1,2.
(2) Solodovnikov, V. D. *Microencapsulation*; Khimia: Moscow, 1980.
(3) Rish, S. J.; Reineccius, G. A. *Encapsulation and controlled release of food ingredients*; ACS Symposium Series 590; American Chemical Society; Washington, DC, 1995.
(4) Stevenson, W. T. K.; Sefton. M. V. *Trends Polym. Sci*. **1994**, *2*, 98.
(5) Rish, R. J.; Reineccius, G. A. *Flavor encapsulation*; ACS Symposium Series 370; American Chemical Society: Washington, DC, 1988.
(6) Greene, L. C.; Meyers, P. A.; Springer, J. T.; Banks, P. A. *J. Agric. Food Chem*. **1992**, *40*, 2274.
(7) Baker, R. W. Controlled release: mechanisms and rates. In *Controlled release of biologically active ingredients*; Tanguary A. C., Lacey, R. E., Eds.; Plenum Press: New York, 1974; p 15.
(8) Giroud, F.; Pernot, J. M.; Brun, H.; Pouyet, B. *J. Microencapsulation* **1995**, *12*, 389.
(9) Donath, E.; Sukhorukov, G. B.; Caruso, F.; Davies, S. F.; Möhwald, H. *Angew. Chem., Int. Ed*. **1998**, *37*, 2702.
(10) Sukhorukov, G. B.; Donath, E.; Lichtenfeld, H.; Knippel, E.; Knippel, M.; Budde, A.; Möhwald, H. *Colloids Surf. A: Physicochem. Eng. Aspects* **1998**, *137*, 253.
(11) Caruso, F.; Yang, W.; Tran, D.; Renneberg, R. *Langmuir* **2000,** *16*, 8932.
(12) Sukhorukov, G. B. Designed Nano-engineered Polymer Films on Colloidal Particles and Capsules. In *Novel Methods to Study Interfacial Layers*; Mobius D., Miller R., Eds.; Elsevier Science B. V.: Amsterdam, 2001; p 383.
(13) Decher, G.; Hong, J. D. *Macromol. Chem. Macromol. Symp*. **1991**, *463*, 21.
(14) Decher, G.; Hong, J. D.; Schmitt, J. *Thin Solid Films* **1992**, *210/211*, 831.
(15) Decher, G. *Science* **1997**, *227*, 1232.
(16) Arys, X.; Jonas, A. M.; Laschewsky, A.; Legras, R. Supramolecular Polyelectrolyte Assemblies. In *Supramolecular Polymers*; Ciferri A., Ed.; Marcel Dekker: New York, 2000; p 505.
(17) Bertrand, P.; Jones, A.; Laschevsky, A.; Legras, R. *Macromol. Rapid Commun*. **2000,** *21*, 319.
(18) Lvov, Y.; Decher, G.; Möhwald, H. *Langmuir* **1993**, *9*, 481.
(19) Mamedov, A. A.; Kotov, N. A. *Langmuir* **2000**, *16*, 5530.
(20) Harris, J. J.; Stair, J. L.; Bruening; M. L. *Chem. Mater*. **2000**, *12*, 1941.
(21) Choi, J. Y.; Rubner, M. F. *J. Macromol. Sci., Pure Appl. Chem.* **2001**, *38*, 1191.
(22) Dubas, S. T.; Schlenoff, J. B. *Macromolecules* **2001**, *34*, 3736.
(23) Ostrander, J. W.; Mamedov, A. A.; Kotov, N, A. *J. Am. Chem. Soc*. **2001**, *123*, 1101.
(24) Lvov, Y.; Price, R.; Gaber, B.; Ischinose, J. *Colloids Surf. A: Physicochem. Eng. Aspects* **2002**, *198*, 375.
(25) Koetse, M.; Laschevsky, A.; Jonas A. M.; Wagenknecht, W. *Langmuir* **2002**, *18*, 1655.
(26) Yang, S. Y.; Rubner, M. F. *J. Am. Chem. Soc*. **2002**, *124*, 2100.
(27) Sukhorukov, G. B.; Antipov, A. A.; Voigt, A.; Donath, E.; Möhwald, H. *Macromol. Rapid Commun*. **2001**, *22*, 44.
(28) Antipov, A. A.; Sukhorukov, G. B.; Leporatti, S.; Radchenko, I. L.; Donath, E.; Möhwald, H. *Colloids Surf. A: Physicochem. Eng. Aspects* **2002**, *198*−*200*, 535.
(29) Moya, S.; Donath, E.; Sukhorukov, G. B.; Auch, M.; Bäumler, H.; Lichtenfeld, H.; Möhwald, H. *Macromolecules* **2000** *33*, 4538.
(30) Sukhorukov, G. B.; Donath, E.; Moya, S.; Susha, A. S.; Voigt, A.; Hartman, J.; Möhwald. H. *J. Microencapsulation* **2000**, *17*, 177.
(31) von Klitzing, R.; Möhwald, H. *Macromolecules* **1996**, *29*, 6901.
(32) Antipov, A. A.; Sukhorukov, G. B.; Donath, E.; Möhwald. H. *J. Phys. Chem*. B **2001**, *105*, 2181.
(33) Qiu, X.; Donath, E.; Möhwald, H. *Macromol. Mater. Eng*. **2001**, *286*, 591.
(34) Krasemann, L.; Tieke, B. *Langmuir* **2000**, *16*, 287.
(35) Dai, J.; Jensen, A. W.; Mahanty, D. K.; Erndt, J.; Bruening, M. L. *Langmuir* **2001**, *17*, 931.
(36) Farhat, T. R.; Schlenoff, J. B. *Langmuir* **2001**, *17*, 1184.
(37) Nernst, W.; Brunner, E. *Z. Phys. Chem*. **1904**, *47*, 52.
(38) Akselrud, G. A.; Molchanov, A. D. *Dissolution of solids*; Khimiya: Moscow, 1977.
(39) Karazhanov, N. A. *Foundations of the kinetics of salts dissolving*; Nauka: Alma-Ata (Kazakh SSR), 1989.
(40) Allen, T. Particle size distribution. In *Powder technology series*; Williams, J. C., Ed.; Chapman and Hall: London, 1975.
(41) Petrov, A. I.; Gavryushkin, A. V. Unpublished results.
(42) Gao, C.; Moya, S.; Lichtenfeld, H.; Casoli, A.; Fiedler, H.; Donath, E.; Möhwald, H. *Macromol. Mater. Eng*. **2001**, *286*, 355.
(43) Georgieva, R.; Moya, S.; Leporatti, S.; Neu, B.; Baumer, H.; Reichle, C.; Donath, E.; Möhwald, H. *Langmuir* **2000**, *16*, 7075.
(44) Harries, J. J.; Bruening, M. L. *Langmuir* **2000**, *16*, 2006.
(45) Ersoz, M. *J. Colloid Interface Sci*. **2000**, *232*, 340.